J. Ocean Univ. China (Oceanic and Coastal Sea Research)
https://doi.org/10.1007/s11802-019-3950-2
ISSN 1672-5182, 2019 18 (4): 771-783
http://www.ouc.edu.cn/xbywb/
E-mail:xbywb@ouc.edu.cn

Analytical Solution for 3D Tidal Flow with Vertically Varying Eddy Viscosity

CHEN Yang[1)], JIANG Wensheng[1), 2), *], and FENG Shizuo[1), 2)]

1) *Physical Oceanography Laboratory/CIMST*, *Ocean University of China and Qingdao National Laboratory for Marine Science and Technology*, *Qingdao* 266100, *China*
2) *Laboratory of Marine Environment and Ecology*, *Ocean University of China*, *Qingdao* 266100, *China*

(Received June 27, 2018; revised November 28, 2018; accepted January 19, 2019)

Abstract In this study, a 3D idealized model of tidal flow, in which the tidal elevation and velocities are solved analytically, is developed. The horizontal eddy viscosity is neglected, and the vertical eddy viscosity used in the study is assumed to be independent of time and only varies as a parabolic function in the vertical direction. The analytical solution is obtained in a narrow rectangular bay, with the topography varying only across the bay. The model results are compared with the field observations in the Xiangshan Bay. The results show that the influence of varying vertical eddy viscosity mainly has two aspects. On one hand, it amplifies the magnitude of the tidal elevation, particularly the amplitude near the head of the bay. On the other hand, it adjusts the axial velocity profile, resulting in an obvious frictional effect. Furthermore, the tidal elevation and velocities are more sensitive to the magnitude of the eddy viscosity near the bottom than the structure in the upper water layer.

Key words vertically varying eddy viscosity; tidal flow; analytical solution; three dimensional

1 Introduction

The tide is often the dominant process in shallow seas and bays and plays an important role in mass transport and water mixing. Therefore, it is essential to understand tidal motion accurately, which is meaningful to oceanography and ocean engineering.

Many studies of the tide and tidal current can be broadly divided into two categories: numerical models, which are appropriate for detailed studies of tidal flow in realistic settings, and analytical solutions, which consider only the dominant factors with simplified geometric profiles.

Early numerical models are mainly horizontal 2D models (An, 1977; Choi, 1980; Fang *et al*., 1984; Fang and Yang, 1985; Carbajal and Backhaus, 1998). The 2D models can reproduce the surface elevation well but cannot obtain information about the vertical velocity profiles, thus prompting the transition from 2D models to 3D models. For example, Jan *et al*. (2004) adopted a tidal model, in which the vertical eddy viscosity is constant everywhere. Meanwhile, Guo and Yanagi (1998) and Warner *et al*. (2005) simulated tidal current by using different turbulence closure methods. It seems that tidal flow can be solved on the basis of such studies mentioned previously. However, Davies and Gerritsen (1994) and Guo and Yanagi (1998) pointed out that the closure schemes for eddy viscosity are crucial to the accuracy of the model results.

Analytical solutions that rely on simple formulations of vertical eddy viscosity have been used to investigate tidal motion for a long time. In most cases, the breadth-averaged 2D model was used with a constant (Wang and Craig, 1993; Li and Valle-Levinson, 1999) or parameterized horizontally varying vertical eddy viscosity (Chernetsky *et al*., 2010). For example, Ianniello (1977) used the breadth-averaged 2D model with a vertically varying vertical eddy viscosity. For 3D solutions, Li (2001) presented a solution for tides in channels to show the effect of bathymetry and friction with a constant eddy viscosity. Winant (2007) obtained a more typical 3D result by analytically studying the tidal flow in an elongated rectangular bay with a constant eddy viscosity. Ensing *et al*. (2015) expanded the model of Winant (2007) by including the exponentially decaying width, and Ross *et al*. (2017) made further modifications to investigate the effect of channel width convergence and friction on tidal flow, in which the vertical eddy viscosity is a constant again.

Summarizing the previously mentioned studies, it is clear that, currently, there is no analytical model of 3D tidal motion that considers the spatially varying vertical eddy viscosity. The horizontal eddy viscosity is considered to have only a slight influence on tide (*e.g.*, Davies *et al*., 1997), whereas the vertical eddy viscosity that

* Corresponding author. Tel: 0086-532-66782977
E-mail: wsjang@ouc.edu.cn

represents the interior friction of the tidal current has a considerable effect on tidal flow. Although the vertical eddy viscosity has no uniform profile, field observations indicate that the vertical eddy viscosity roughly follows a parabolic form, with a small value near the bottom and approximately reaching the maximum value near mid-depth (Bowden *et al*., 1959; Lu and Lueck, 1999; Xu *et al*., 2013). A numerical research that used a turbulence closure model in a narrow bay also obtained a similar profile of tidally averaged vertical eddy viscosity (Deng *et al*., 2017).

In this study, a 3D analytical tidal model with spatially varying vertical eddy viscosity is solved in a narrow bay. The vertical eddy viscosity is regarded as a function of the vertical coordinate only and follows a parabolic form according to Ianniello (1977) who used a 2D flat-bottom analytical model to investigate the tide-induced residual current and according to Tee (1979) who adopted a 3D numerical model to analyze the tidal current. This study mainly aims to improve the analytical solution for tidal flow by involving the spatially varying eddy viscosity and to understand the influence of the spatially varying vertical eddy viscosity on the 3D tidal flow analytically. The analytical solution can also be the benchmark for the validation of the numerical model.

The paper is organized as follows: The formulation of the model is given in Section 2. The solution procedure of tidal flow is described in Section 3. The results and comparisons are presented in Section 4. The discussions are made in Section 5. The conclusions are drawn in Section 6.

2 Formulation

Winant (2007) solved the 3D tidal motion in a narrow bay analytically under weakly nonlinear assumptions. Jiang and Feng (2014) eliminated the unnecessary hypothesis and revisited the problem by using the double perturbation method in analyzing the residual current. In this study, the framework of the model follows those of Winant (2007) and Jiang and Feng (2014), and the solution procedure follows that of Jiang and Feng (2014).

2.1 The Non-Dimensional Tidal Equations

In this study, the 3D tidal current in a semi-enclosed rectangular bay will be solved. The x and y coordinates are along the two horizontal sides of the bay with $x=0$ being at the open boundary and $x=L$ being at the head of the bay. The lateral boundaries are $y=y_b$ and $y=y_e$. The surface of still water is set at $z=0$, and the sea bottom is set at $z=-h$. The tidal signal is imposed at the open boundary so the tidal current is the main movement in the area.

We assume that the variables have the following characteristic values: $x_c=\lambda$, $y_c=B$, $z_c=h_c$, and $t_c=2\pi/\omega_c$, where $\lambda=\sqrt{gh_c/\omega_c}$ is the wavelength, h_c is the typical water depth of the sea area, ω_c is the circular frequency of the tide, and ζ_c is the characteristic value of tidal elevation.

Given the basic balance of tidal movement $O\left(\frac{\partial u}{\partial t}\right)=O\left(g\frac{\partial \zeta}{\partial x}\right)$, the characteristic value of u has the following relation: $u_c=\zeta_c\sqrt{g/h_c}$. If the continuity equation is considered, then the characteristic values of v and w can be obtained, *i.e.*, $v_c=B\zeta_c\omega_c/h_c$ and $w_c=\zeta_c\omega_c$.

Then, the nondimensional form of the governing equations can be expressed as follows:

$$\nabla\cdot\boldsymbol{u}=0, \tag{1}$$

$$\frac{\partial u}{\partial t}+\kappa\boldsymbol{u}\cdot\nabla u=-\frac{\partial\zeta}{\partial x}+\beta\frac{\partial}{\partial z}\left(\upsilon\frac{\partial u}{\partial z}\right), \tag{2}$$

$$\delta^2\frac{\partial v}{\partial t}+\kappa\delta^2\boldsymbol{u}\cdot\nabla v=-\frac{\partial\zeta}{\partial y}+\beta\delta^2\frac{\partial}{\partial z}\left(\upsilon\frac{\partial v}{\partial z}\right), \tag{3}$$

where $\delta=B/\lambda$, $\kappa=\zeta_c/h_c$, and $\beta=\left(\sqrt{\upsilon_c/\omega_c}/h_c\right)^2$, with υ_c being the characteristic value of the vertical eddy viscosity.

At the sea surface, $z=\kappa\zeta$,

$$\begin{cases} w=\dfrac{\partial\zeta}{\partial t}+\kappa\left(u\dfrac{\partial\zeta}{\partial x}+v\dfrac{\partial\zeta}{\partial y}\right) \\ \dfrac{\partial(u,v)}{\partial z}=0 \end{cases}. \tag{4}$$

At the sea bottom, $z=-h$,

$$\boldsymbol{u}=0. \tag{5}$$

At the fixed boundary,

$$\begin{cases} \int_{-h}^{\kappa\zeta}v\mathrm{d}z=0 \text{ at } y=y_b \text{ and } y_e \\ \int_{-h}^{\kappa\zeta}u\mathrm{d}z=0 \text{ at } x=L \end{cases}. \tag{6}$$

At the open boundary, $x=0$,

$$\zeta=\zeta_{\text{open}}. \tag{7}$$

Thus, Eqs. (1) to (7) define a non-dimensional system of 3D tidal flow. The entire system has two basic dimensionless numbers. One is κ, the tidal amplitude over the average water depth, which reflects the nonlinear effect of the system. The other is δ, the aspect ratio, which reflects the asymmetric feature of the horizontal geometry of the model area. In the present study, the case of $O(\kappa)<1$ and $O(\delta)<1$ is investigated, which indicates that tidal motion is a weakly nonlinear case in a narrow bay, in which the Coriolis effect is negligible.

2.2 The Perturbation in a Narrow Bay

To solve the tidal equations, the double-perturbation method is used to expand the tidal equations with small parameters κ and δ^2. The equations of different orders

used to solve the zeroth-order tidal current are listed in Subsection 2.2.1, and the details of the mathematical procedures used to obtain these equations are shown in Appendix A.

2.2.1 The zeroth-order equations

$$\nabla\cdot\boldsymbol{u}_0=0\ , \tag{8}$$

$$\frac{\partial u_0}{\partial t}=-\frac{\partial\zeta_0}{\partial x}+\beta\frac{\partial}{\partial z}\left(\upsilon\frac{\partial u_0}{\partial z}\right), \tag{9}$$

$$0=-\frac{\partial\zeta_0}{\partial y}\ . \tag{10}$$

At the sea surface, $z=0$,

$$\begin{cases} w_0=\dfrac{\partial\zeta_0}{\partial t} \\ \dfrac{\partial(u_0,v_0)}{\partial z}=0 \end{cases}. \tag{11}$$

At the sea bottom, $z=-h$,

$$\boldsymbol{u}_0=0\ . \tag{12}$$

At the fixed boundary,

$$\begin{cases} \int_{-h}^{0}v_0\mathrm{d}z=0 \text{ at } y=y_b \text{ and } y_e \\ \int_{-h}^{0}u_0\mathrm{d}z=0 \text{ at } x=L \end{cases}. \tag{13}$$

At the open boundary, $x=0$,

$$\zeta_0=\zeta_{\text{open}}\ . \tag{14}$$

3 The Solution for Tidal Flow

When the non-dimensional eddy viscosity is assumed to be independent of time, the zeroth-order tidal current system (*i.e.*, Eqs. (8) to (14)) can be solved analytically by considering the $O(\delta^2)$ order momentum equation in the y-direction:

$$\frac{\partial v_0}{\partial t}=-\frac{\partial\zeta_0'}{\partial y}+\beta\frac{\partial}{\partial z}\left(\upsilon\frac{\partial v_0}{\partial z}\right). \tag{15}$$

Given that the zeroth-order equations are linear and the open boundary condition is given as a single frequency tide, the solutions should be periodic. Thus, the solutions can be assumed to have the following forms:

$$u_0=\mathrm{Re}[U_0\mathrm{e}^{-it}],\ \ v_0=\mathrm{Re}[V_0\mathrm{e}^{-it}],\ \ \ w_0=\mathrm{Re}[W_0\mathrm{e}^{-it}],$$

$$\zeta_0=\mathrm{Re}[N_0\mathrm{e}^{-it}],\ \ \zeta_0'=\mathrm{Re}[N_0'\mathrm{e}^{-it}],$$

where U_0, V_0, and W_0 are the functions of (x, y, z) and N_0 is the function of (x, y) only. *i.e.*

After the substitution of these equations into the momentum equations (*i.e.*, Eqs. (9) and (10)), the following relations can be obtained:

$$-iU_0=-\frac{\partial N_0}{\partial x}+\beta\frac{\partial}{\partial z}\left(\upsilon\frac{\partial U_0}{\partial z}\right), \tag{16}$$

$$0=-\frac{\partial N_0}{\partial y}\ . \tag{17}$$

Then, N_0 is independent of y and is a function of x only, which can be denoted as $N_0(x)$. Thus, the momentum equation (*i.e.*, Eq. (15)) can be rewritten as follows:

$$-iV_0=-\frac{\partial N_0'}{\partial y}+\beta\frac{\partial}{\partial z}\left(\upsilon\frac{\partial V_0}{\partial z}\right), \tag{18}$$

and the boundary conditions of Eqs. (16) and (18) can be expressed as follows:

$$\begin{cases} \dfrac{\partial U_0}{\partial z}=\dfrac{\partial V_0}{\partial z}=0 \text{ at } z=0 \\ U_0=V_0=0 \text{ at } z=-h \end{cases}, \tag{19}$$

$$\begin{cases} \int_{-h}^{0}U_0\mathrm{d}z=0 \text{ at } x=L \\ \int_{-h}^{0}V_0\mathrm{d}z=0 \text{ at } y=y_b \text{ and } y_e \end{cases}. \tag{20}$$

3.1 The Solution for the Momentum Equations

With the non-dimensional vertical eddy viscosity being regarded as a function of z only, the Eqs. (16) and (18) can be expanded as follows:

$$\upsilon(z)\frac{\partial^2U_0}{\partial z^2}+\frac{\partial\upsilon(z)}{\partial z}\frac{\partial U_0}{\partial z}+\frac{i}{\beta}U_0=\frac{1}{\beta}\frac{\partial N_0}{\partial x}\ , \tag{21}$$

$$\upsilon(z)\frac{\partial^2V_0}{\partial z^2}+\frac{\partial\upsilon(z)}{\partial z}\frac{\partial V_0}{\partial z}+\frac{i}{\beta}V_0=\frac{1}{\beta}\frac{\partial N_0'}{\partial y}\ . \tag{22}$$

According to Ianniello (1977), $\upsilon(z)$ can be further assumed to have the following parabolic form:

$$\upsilon(z)=a_1(z+a_2)(z+a_3)\ , \tag{23}$$

where

$$a_1=-\frac{1-R}{(z_m+h_0)^2}\ ,$$

$$a_2=-z_m+(z_m+h_0)\left(\frac{1}{1-R}\right)^{1/2},$$

$$a_3=-z_m-(z_m+h_0)\left(\frac{1}{1-R}\right)^{1/2}.$$

As shown in Fig.1, υ has the minimum value of R ($0<R<1$) at $z=-h_0$ and attains its maximum value of 1 at $z=z_m=-h_0h_m$, where h_0 is the maximum value of the water depth, which is 1 in the non-dimensional condition, and $h_m<1/2$ is assumed according to the real situation.

After the substitution of Eq. (23) into Eqs. (21) and (22), the following relations can be obtained:

$$a_1(z+a_2)(z+a_3)\frac{\partial^2 U_0}{\partial z^2}+ a_1(2z+a_2+a_3)\frac{\partial U_0}{\partial z}+\frac{i}{\beta}U_0=\frac{1}{\beta}\frac{\partial N_0}{\partial x}, \quad (24)$$

$$a_1(z+a_2)(z+a_3)\frac{\partial^2 V_0}{\partial z^2}+ a_1(2z+a_2+a_3)\frac{\partial V_0}{\partial z}+\frac{i}{\beta}V_0=\frac{1}{\beta}\frac{\partial N_0'}{\partial y}. \quad (25)$$

To obtain the solutions to Eqs. (24) and (25), a coordinate transformation is introduced and the equations can be converted into non-homogeneous hypergeometric equations. On the basis of the properties of the standard hypergeometric functions (Wang and Guo, 2000), the solutions to Eqs. (24) and (25) can be derived as follows

$$U_0(x,y,z)=iq\frac{\partial N_0}{\partial x}, \quad (26)$$

$$V_0(x,y,z)=iq\frac{\partial N_0'}{\partial y}. \quad (27)$$

The expression of q and the details of the solution procedure are shown in Appendix B.

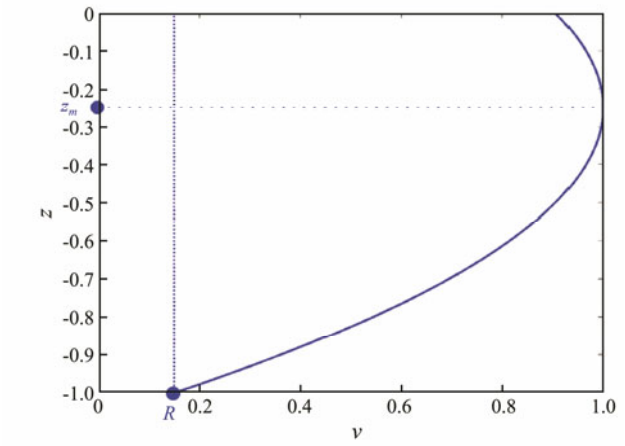

Fig.1 The profile of the non-dimensional vertical eddy viscosity.

3.2 The Solution for the Continuity Equation

When the water depth is considered to vary only along the lateral direction, the continuity equation can be solved using the same method as that used by Winant (2007) and Jiang and Feng (2014). The horizontal velocity is related to the sea surface elevation gradients in Eqs. (26) and (27). Then, the horizontal velocity is inserted into the depth-integrated form of the continuity equation to derive the equation for sea surface elevation. By solving this equation, the sea surface elevation can be obtained as follows

$$N_0=\frac{\cos(\mu(L-x))}{\cos(\mu L)}, \quad (28)$$

where $\mu^{-2}=-\int_0^1 P_0\mathrm{d}y$ is a constant and $P_0=\int_{-h}^0 q\mathrm{d}z$.

The following equation can also be obtained,

$$\frac{\partial N_0'}{\partial y}=\frac{G}{P_0}\frac{\partial^2 N_0}{\partial x^2}, \quad (29)$$

where $G=-\int_0^y P_0(y')\mathrm{d}y'-y\mu^{-2}$.

Then, the zeroth-order velocities U_0, V_0 and W_0 can be expressed as follows,

$$U_0=\frac{i\mu\sin(\mu(L-x))}{\cos(\mu L)}q, \quad (30)$$

$$V_0=-\frac{i\mu^2 G\cos(\mu(L-x))}{P_0\cos(\mu L)}q, \quad (31)$$

$$W_0=\frac{i\mu^2\cos(\mu(L-x))}{\cos(\mu L)}\cdot \left[-\left(\frac{\mu^{-2}}{P_0}+\frac{G}{P_0^2}\frac{dP_0}{dy}\right)\int_{-h}^z q\mathrm{d}z'+\frac{G}{P_0}\int_{-h}^z\frac{\partial q}{\partial y}\mathrm{d}z'\right]. \quad (32)$$

Thus, the tidal elevation and velocities with spatially varying eddy viscosity are obtained analytically. The parameters that control the solutions are as follows: β is the quadratic ratio of the frictional depth ($h_d=\sqrt{\upsilon_c/\omega_c}$) and the undisturbed water depth (h_c), R and h_m together decide the vertical eddy viscosity, and L is the length of the bay relative to the tidal wavelength.

4 Results

The solution for a bay with the water depth varying along the transverse direction can be expressed as follows:

$$h=1-0.99(2y-1)^2.$$

The length of the bay is set 1.5 times of the wavelength with fixed values of R and h_m. The phase and amplitude of N_0 are presented in Fig.2. When β is small, the minimum point of the amplitude is observed near the open boundary. As β increases, the minimum point moves toward the head of the bay. When β is large, the minimum point is not apparent anymore. The amplitude near the head decreases with the increase in β. Meanwhile, the phase decreases gradually with the increase in β.

According to the definition, β represents the magnitude of the vertical eddy viscosity, whereas R and h_m together decide the specific profile of the non-dimensional vertical eddy viscosity, which is different from that of the constant eddy viscosity condition. The tidal elevation obtained with varying vertical eddy viscosity is compared with that obtained with constant eddy viscosity ($\upsilon=1$) when the

value of β is kept constant. The results show that the trend is mainly consistent but exhibits a distinct difference in magnitude between the present result (solid lines) and that with the constant eddy viscosity (dashed lines). In the present results, the minimum point of the amplitude is close to the open boundary, and the amplitude near the head increases apparently. The relative variation rates of the amplitude between constant and varying eddy viscosities at the head of the bay for $\beta=0.02$, 0.125, and 0.5 are 11%, 24%, and 66%, respectively. The vertically varying eddy viscosity also leads to a general increase in phase, and the relative variation rates in the middle of the bay for $\beta=0.02$, 0.125, and 0.5 are 3%, 9%, and 11%, respectively.

Fig.3 shows the velocities at six tidal phases starting from the phase of high water in the middle of the bay with three different values of β. At high water, the axial velocity u_0 is weak and changes sign. As time progresses, u_0 becomes negative throughout the section, which corresponds to an ebb tide. When β is small, u_0 is nearly

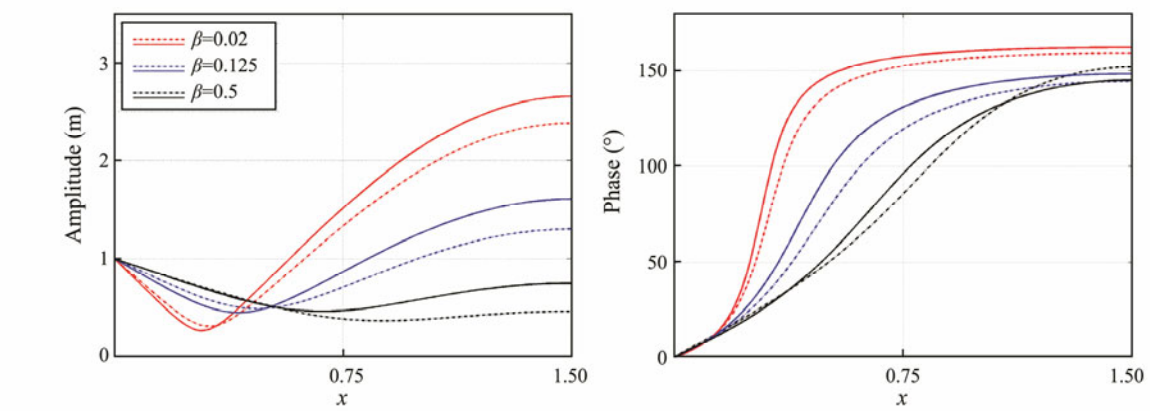

Fig.2 Amplitude and phase of N_0 for three different values of β ($R=0.15$, $h_m=1/4$). Solid and dashed lines represent the results with varying and constant vertical eddy viscosities, respectively.

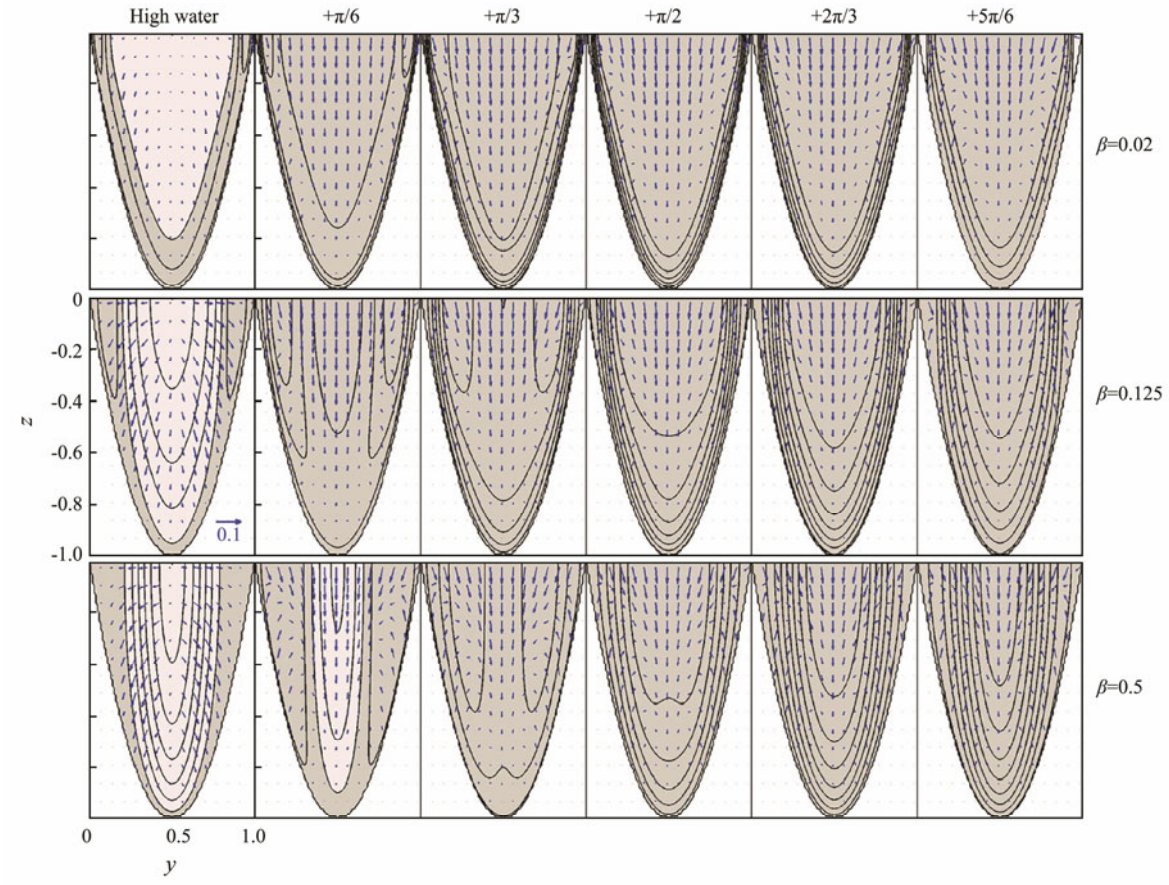

Fig.3 Velocities at six tidal phases for three different values of β ($R=0.15$, $h_m=1/4$). The section is located in the middle of the bay. The leftmost column corresponds to the phase of high water. The axial velocity is negative in the shaded area. The lateral and vertical velocities are represented by arrows.

constant over the section, with the shear confined near the bottom. As β increases, the shear in u_0 will be distributed throughout the entire section, and the lateral and vertical velocities will also increase.

The vertical profiles of u_0 at six phases for three different values of β are presented in Fig.4. The red solid lines represent the results with varying vertical eddy viscosity, and the blue dashed lines represent the results with constant vertical eddy viscosity. With the constant vertical eddy viscosity, the maximum $|u_0|$ is detected only at the surface in the middle of the bay (mid-basin and mid-width) when the value of β is large, and the maximum point submerges when the value of β is small. As shown in Fig.4, the profiles obtained in the present study are better than those of the results with constant vertical eddy viscosity. The maximum $|u_0|$ at the surface is more prominent when the value of β is large, and the maximum point submerges lower as the value of β decreases. Moreover, u_0 is nearly constant over the section with the shear constrained near the bottom, and the frictional effect is more obvious with the varying eddy viscosity.

According to the expression of β presented previously, a small β indicates a relatively small ratio of h_d to h_c. Thus, the frictional effect is limited near the bottom and the rest of the water column is approximately uniform. When β is large, the proportion of h_d increases, resulting in the frictional effect breaking the limit and reaching the middle layer of the water column.

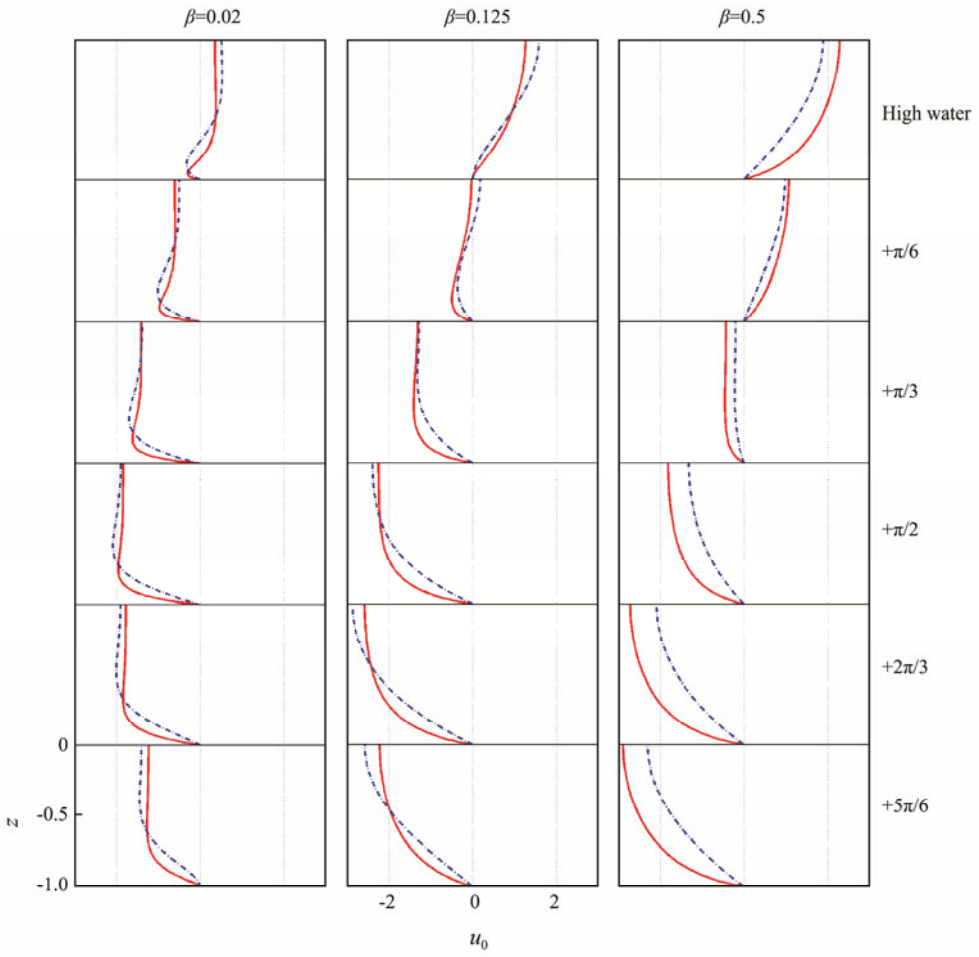

Fig.4 Vertical profiles of u_0 at six tidal phases for three different values of β ($R=0.15$, $h_m=1/4$). The section is located in the middle of the bay. Red solid lines and blue dashed lines represent the results of varying and constant vertical eddy viscosities, respectively.

5 Discussion

5.1 Application in the Xiangshan Bay

To test the applicability of the solution, the analytical model is applied in the Xiangshan Bay and the results of the tidal elevation and velocities are compared with the field data.

The Xiangshan Bay is a semi-enclosed bay in Zhejiang Province, China. The bay is approximately 70 km long and 10 km wide, with an average depth of approximately 10 m. The bay is characterized by a dominant M_2 tide with limited freshwater input and weak wind. The bathymetry of the entire bay is rather complex, *i.e.*, the outer part is wide with large mudflats, whereas the inner part is narrow. The field data were obtained at three stations (Quan, 2014; Xu *et al.*, 2016, 2017), as shown in Fig.5. Station B1 is near the head of the bay, and station

B2 is approximately 5 km away from station B1. The tidal elevation and current profile data were collected at the two stations from 11:00 AM, December 19, 2012 to 12:00 AM, December 20, 2012 using the bottom-mounted ADCP and the RBR XR420 CTD. Station D1 is near the open boundary, where the tidal elevation data were collected for 25 h.

The crude idealization of the Xiangshan Bay is 70 km long and 10 m deep. The characteristic value of the vertical eddy viscosity was set at $\upsilon_c = 5.5\times10^{-3}\ \mathrm{m^2\,s^{-1}}$. Thus, the M_2 tide in the Xiangshan Bay is represented by non-dimensional parameters $\beta = 0.39$ and $L = 0.16$ in the model. The simulated amplitude and phase of N_0 obtained using the analytical model are compared with the M_2 harmonic constants obtained by analyzing the observational data of tidal elevation at the three stations. As shown in Fig.6, the analytical results are consistent with the field results and are capable of reproducing the tidal elevation well. The simulated axial velocity profiles at three main tidal phases are compared with the velocity profiles obtained at stations B1 and B2 in Fig.7. Notably, the simulated velocity profiles generally follow the tendency of the measured profiles from the surface to the lower layer, except for an apparent difference near the bottom. This finding reflects a limitation of the analytical model, *i.e.*, it cannot represent the complex reality, such as the no-slip bottom condition used in the analytical model.

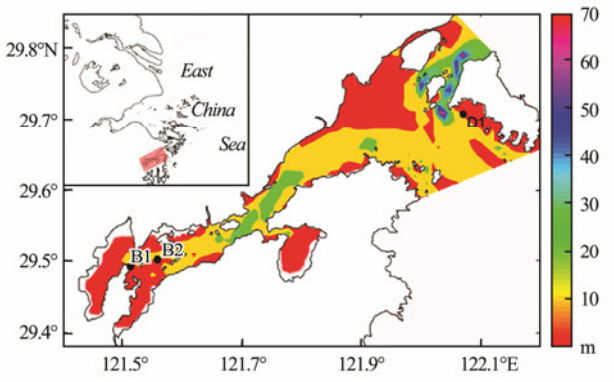

Fig.5 The location and bathymetry of the Xiangshan Bay. The black dots mark the observational stations B1, B2, and D1. At stations B1 and B2, the tidal elevation and current profile data were collected. At station D1, only the tidal elevation data were collected.

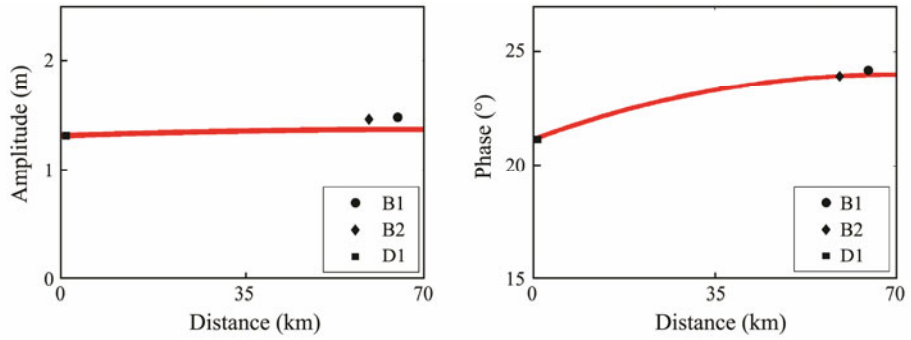

Fig.6 Simulated amplitude and phase of N_0 for the M_2 tide in the Xiangshan Bay (red lines, $R = 0.3$, $h_m = 1/4$) compared with the harmonic constants analyzed from field data (black marks).

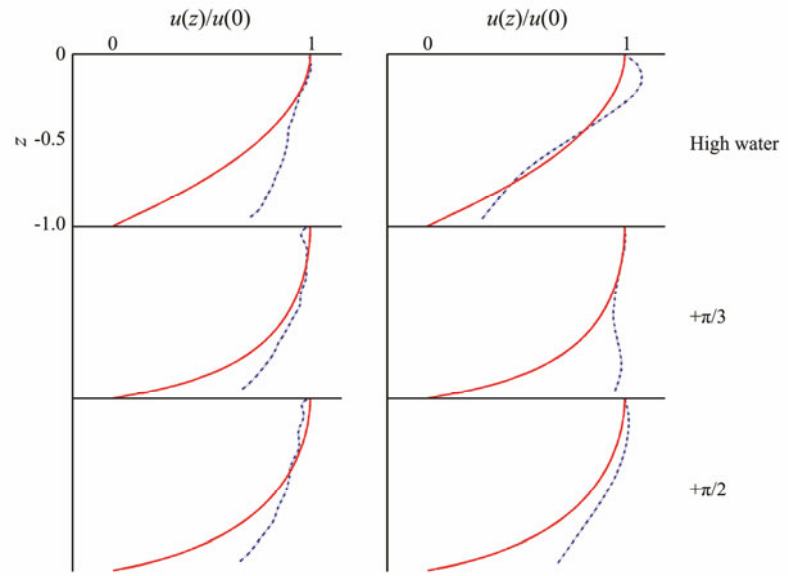

Fig.7 Comparison between simulated (red solid lines, $R = 0.3$, $h_m = 1/4$) and measured (blue dashed lines) axial velocity profiles at three tidal phases for stations B1 (left panel) and B2 (right panel).

5.2 Sensitivity to the Vertical Eddy Viscosity

The present study adopted a parabolic form for the vertical eddy viscosity, as proposed in many studies. As discussed in Section 3.1, the vertical eddy viscosity υ is a function of two non-dimensional parameters, *i.e.*, R and h_m. R is the value of υ near the bottom, which determines the mean value of υ. h_m is the vertical position of the maximum υ, which represents the structure of υ in the upper water layer. The sensitivity of the tidal elevation and velocities to the structure of the vertical eddy viscosity is examined by changing the values of R and h_m.

Control experiments are conducted to determine the effects of R and h_m. In Fig.8, the amplitude and phase of N_0 is drawn for different values of R and h_m. As R increases, the minimum point of the amplitude slightly moves toward the head of the bay and the maximum amplitude decreases, as well as the phase. The increase in the value of h_m has the same effect, but the change is minimal. For the axial tidal velocities (Fig.9), the ratio of $u(z)/u(0)$ decreases with the increase in the value of R but is insensitive to the variation of h_m.

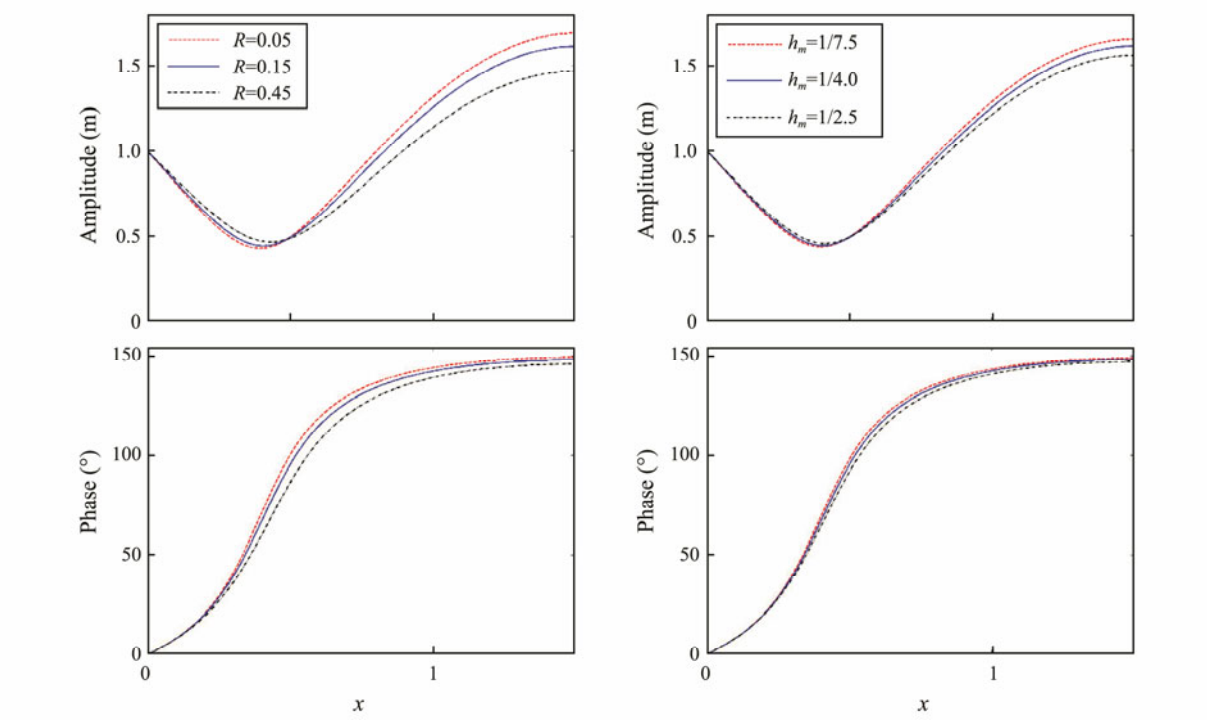

Fig.8 Amplitude and phase of N_0 for different R (left panel) and h_m (right panel) values, with $\beta = 0.125$.

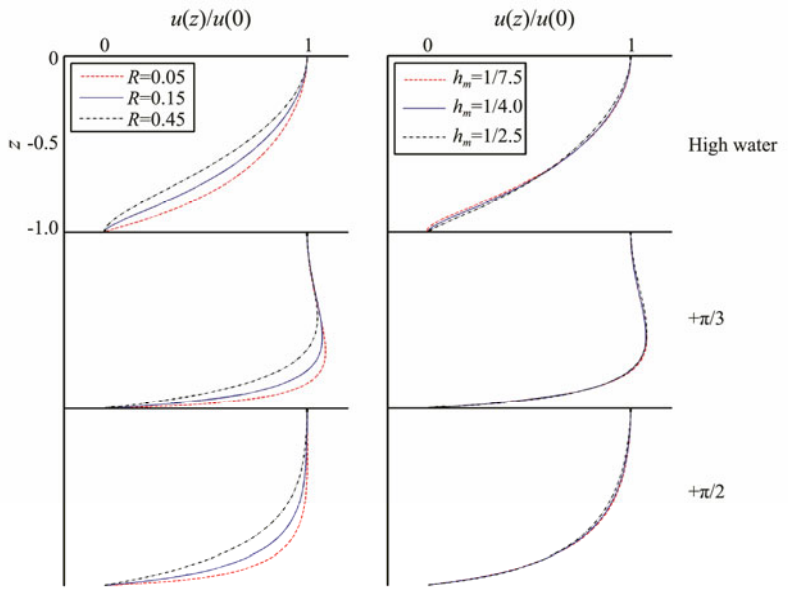

Fig.9 Vertical distributions of $u(z)/u(0)$ at three tidal phases for different R (left panel) and h_m (right panel) values, with a moderate value of $\beta = 0.125$.

These results indicate that the tidal elevation and velocities are more sensitive to R (the value of the eddy viscosity near the bottom) than h_m (the structure in the upper water layer). This finding is consistent with the result of Ianniello (1977) who examined the velocity profiles for a wide range of R and h_m in a breadth-averaged 2D idealized bay. The results of the sensitivity test can be explained by the findings presented in Section 4. With a certain tidal frequency, the characteristic value of vertical eddy viscosity decides h_d, *i.e.*, the frictional effect. This frictional effect is often limited in the lower layer of the water column or even near the bottom. Thus, the vertical eddy viscosity near the bottom (R) that decides the mean value of υ is important, and the specific structure of υ in the upper water layer (h_m) is insignificant.

6 Conclusions

A 3D idealized model of a semi-enclosed narrow bay with depth varying along the lateral direction has been developed. The 3D tidal flow with the vertical eddy viscosity varying with z is solved analytically.

For a narrow bay with a given depth profile and length, three parameters control the solution. β is the quadratic ratio of the frictional depth and the undisturbed water depth, which measures the importance of friction. R and h_m together decide the profile of the vertical eddy viscosity.

The results show that the patterns of tidal elevation and velocities are consistent with previous analytical solutions with constant vertical eddy viscosity. The influence of varying vertical eddy viscosity mainly involves amplifying the magnitude of the tidal elevation and adjusting the axial velocity profile.

With the varying vertical eddy viscosity and a moderate value of β, the amplitude of the tidal elevation near the head of the bay has a variation rate larger than 20%. Meanwhile, the variation rate of the phase in the middle of the bay is approximately 10%. The frictional effect on the axial velocity profile is more obvious under the varying vertical eddy viscosity than that under the constant vertical eddy viscosity.

The analytical model is applied in Xiangshan Bay, China, using parameters generalized from the real condition. The model shows that the calculated tidal elevation and axial velocity profiles are consistent with the field results.

The results of the control experiments indicate that the tidal elevation and velocities are more sensitive to the magnitude of the eddy viscosity near the bottom than the detailed structure in the upper water layer, which is consistent with the findings of prior studies.

Thus far, the results show that the present analytical solution is appropriate. The main limitation is that the vertical eddy viscosity used is constant and independent of time. The influence of the time-varying eddy viscosity may be important but is beyond the scope of the present study and needs further investigation.

Acknowledgements

This study was supported by the National Natural Science Foundation of China (No. 41676003) and NSFC-Shandong Joint Fund for Marine Science Research Centers (No. U1606402).

Appendix A: The Perturbation in a Narrow Bay

If the weakly nonlinear case in a narrow bay is considered, then κ and δ are small parameters. We assume that the following equations hold for the expansion with regard to κ and δ^2,

$$\boldsymbol{u}=\boldsymbol{u}_0+\kappa\boldsymbol{u}_1+\delta^2\boldsymbol{u}_0'+\kappa\delta^2\boldsymbol{u}_1'+\cdots, \tag{33}$$

$$\zeta=\zeta_0+\kappa\zeta_1+\delta^2\zeta_0'+\kappa\delta^2\zeta_1'+\cdots. \tag{34}$$

The substitution of Eqs. (33) and (34) into Eqs. (1) to (7) ensures that the perturbation equations are accurate to the order of $O(\kappa\delta^2)$,

$$\nabla\cdot\boldsymbol{u}_0+\kappa\nabla\cdot\boldsymbol{u}_1+\delta^2\nabla\cdot\boldsymbol{u}_0'+\kappa\delta^2\nabla\cdot\boldsymbol{u}_1'=0, \tag{35}$$

$$\frac{\partial u_0}{\partial t}+\kappa\left(\frac{\partial u_1}{\partial t}+\boldsymbol{u_0}\cdot\nabla u_0\right)+\delta^2\frac{\partial u_0'}{\partial t}+\kappa\delta^2\left(\frac{\partial u_1'}{\partial t}+\boldsymbol{u_0}\cdot\nabla u_0'+\boldsymbol{u_0'}\cdot\nabla u_0\right)=$$
$$-\frac{\partial\zeta_0}{\partial x}+\beta\frac{\partial}{\partial z}\left(\upsilon\frac{\partial u_0}{\partial z}\right)+\kappa\left[-\frac{\partial\zeta_1}{\partial x}+\beta\frac{\partial}{\partial z}\left(\upsilon\frac{\partial u_1}{\partial z}\right)\right]+\delta^2\left[-\frac{\partial\zeta_0'}{\partial x}+\beta\frac{\partial}{\partial z}\left(\upsilon\frac{\partial u_0'}{\partial z}\right)\right]+\kappa\delta^2\left[-\frac{\partial\zeta_1'}{\partial x}+\beta\frac{\partial}{\partial z}\left(\upsilon\frac{\partial u_1'}{\partial z}\right)\right], \tag{36}$$

$$\delta^2\frac{\partial v_0}{\partial t}+\kappa\delta^2\left(\frac{\partial v_1}{\partial t}+\boldsymbol{u}_0\cdot\nabla v_0\right)=-\frac{\partial\zeta_0}{\partial y}-\kappa\frac{\partial\zeta_1}{\partial y}+\delta^2\left[\beta\frac{\partial}{\partial z}\left(\upsilon\frac{\partial v_0}{\partial z}\right)-\frac{\partial\zeta_0'}{\partial y}\right]+\kappa\delta^2\left[\beta\frac{\partial}{\partial z}\left(\upsilon\frac{\partial v_1}{\partial z}\right)-\frac{\partial\zeta_0'}{\partial y}\right]. \tag{37}$$

Given that the sea surface is set at

$$z=\kappa(\zeta_0+\kappa\zeta_1+\delta^2\zeta_0'+\kappa\delta^2\zeta_1'),$$

the Taylor expansion will be used to transfer the boundary conditions to $z=0$, as follows,

$$u|_{z=\zeta}=u|_{z=0}+\kappa(\zeta_0+\kappa\zeta_1+\delta^2\zeta_0'+\kappa\delta^2\zeta_1')u_z|_{z=0}+$$
$$1/2\kappa^2(\zeta_0+\kappa\zeta_1+\delta^2\zeta_0'+\kappa\delta^2\zeta_1')^2u_{zz}|_{z=0},$$

$$\upsilon|_{z=\zeta}=v|_{z=0}+\kappa(\zeta_0+\kappa\zeta_1+\delta^2\zeta_0'+\kappa\delta^2\zeta_1')\upsilon_z|_{z=0}+$$
$$1/2\kappa^2(\zeta_0+\kappa\zeta_1+\delta^2\zeta_0'+\kappa\delta^2\zeta_1')^2v_{zz}|_{z=0},$$

$$w|_{z=\zeta}=w|_{z=0}+\kappa(\zeta_0+\kappa\zeta_1+\delta^2\zeta_0'+\kappa\delta^2\zeta_1')w_z|_{z=0}+$$

$$1/2\kappa^2(\zeta_0+\kappa\zeta_1+\delta^2\zeta_0'+\kappa\delta^2\zeta_1')^2 w_{zz}|_{z=0}.$$

This relation can be inserted into the surface condition to obtain the following boundary conditions at $z=0$,

$$w_0+\kappa\left(w_1+\frac{\partial w_0}{\partial z}\zeta_0\right)+\delta^2 w_0'+\kappa\delta^2\left(w_1'+\frac{\partial w_0}{\partial z}\zeta_0'+\frac{\partial w_0'}{\partial z}\zeta_0\right)=$$
$$\frac{\partial\zeta_0}{\partial t}+\kappa\left(\frac{\partial\zeta_1}{\partial t}+u_0\frac{\partial\zeta_0}{\partial x}+v_0\frac{\partial\zeta_0}{\partial y}\right)+\delta^2\frac{\partial\zeta_0'}{\partial t}+\kappa\delta^2\left(\frac{\partial\zeta_1'}{\partial t}+u_0\frac{\partial\zeta_0'}{\partial x}+v_0\frac{\partial\zeta_0'}{\partial y}+u_0'\frac{\partial\zeta_0}{\partial x}+v_0'\frac{\partial\zeta_0}{\partial y}\right), \quad (38)$$

and

$$\left[\kappa\delta^2\left(\frac{\partial^2 u_0}{\partial z^2}\zeta_0'+\frac{\partial^2 u_0'}{\partial z^2}\zeta_0+\frac{\partial u_1'}{\partial z}\right)+\kappa\left(\frac{\partial^2 u_0}{\partial z^2}\zeta_0+\frac{\partial u_1}{\partial z}\right)+\delta^2\frac{\partial u_0'}{\partial z}+\frac{\partial u_0}{\partial z},\right.$$
$$\left.\kappa\delta^2\left(\frac{\partial^2 v_0}{\partial z^2}\zeta_0'+\frac{\partial^2 v_0'}{\partial z^2}\zeta_0+\frac{\partial v_1'}{\partial z}\right)+\kappa\left(\frac{\partial^2 v_0}{\partial z^2}\zeta_0+\frac{\partial v_1}{\partial z}\right)+\delta^2\frac{\partial v_0'}{\partial z}+\frac{\partial v_0}{\partial z}\right]=0. \quad (39)$$

At the sea bottom, $z=-h$,

$$u_0+\kappa u_1+\delta^2 u_0'+\kappa\delta^2 u_1'=0,$$
$$v_0+\kappa v_1+\delta^2 v_0'+\kappa\delta^2 v_1'=0,$$
$$w_0+\kappa w_1+\delta^2 w_0'+\kappa\delta^2 w_1'=0.$$

At the fixed boundary, $y=y_b$ and y_e,

$$\int_{-h}^{\kappa(\delta^2\kappa\zeta_1'+\delta^2\zeta_0'+\kappa\zeta_1+\zeta_0)}(\delta^2\kappa v_1'+\delta^2 v_0'+\kappa v_1+v_0)\mathrm{d}z=0.$$

This expression can be rewritten as follows.

$$\int_{-h}^{0}(\delta^2\kappa v_1'+\delta^2 v_0'+\kappa v_1+v_0)\mathrm{d}z+$$
$$\kappa(\delta^2\kappa\zeta_1'+\delta^2\zeta_0'+\kappa\zeta_1+\zeta_0)(\delta^2\kappa v_1'+\delta^2 v_0'+\kappa v_1+v_0)|_{z=0}=0.$$

At the fixed boundary, $x=L$,

$$\int_{-h}^{\kappa(\delta^2\kappa\zeta_1'+\delta^2\zeta_0'+\kappa\zeta_1+\zeta_0)}(\delta^2\kappa u_1'+\delta^2 u_0'+\kappa u_1+u_0)\mathrm{d}z=0.$$

This expression can be rewritten as follows.

$$\int_{-h}^{0}(\delta^2\kappa u_1'+\delta^2 u_0'+\kappa u_1+u_0)\mathrm{d}z+$$
$$\kappa(\delta^2\kappa\zeta_1'+\delta^2\zeta_0'+\kappa\zeta_1+\zeta_0)(\delta^2\kappa u_1'+\delta^2 u_0'+\kappa u_1+u_0)|_{z=0}=0.$$

At the open boundary, $x=0$,

$$\zeta_0+\kappa\zeta_1+\delta^2\zeta_0'+\kappa\delta^2\zeta_1'=\zeta_{\text{open}}. \quad (40)$$

Then, the equations for different orders can be obtained. For example, the zeroth-order equations are expressed as Eqs. (8) to (14), and the $O(\delta^2)$-order momentum equation in the y-direction is expressed as Eq. (15). The analytical solutions for the zeroth-order tide can be obtained based on these equations.

Appendix B: The Solution Procedure to Eqs. (24) and (25)

We introduce a coordinate transformation in the z-direction, as follows,

$$\xi=\frac{z+a_2}{a_2-a_3}. \quad (41)$$

Thus, the notation of the variables depending on z can also be rewritten, as follows,

$$\tilde{U}(x,y,\xi)=U_0(x,y,z),$$
$$\tilde{V}(x,y,\xi)=V_0(x,y,z),$$

because

$$\frac{1}{a_2-a_3}=\frac{\sqrt{(1-R)}}{2\left(z_m+h_0\right)}>0.$$

Thus, ξ has its minimum value at $z=-h_0$ and reaches its maximum value at $z=0$, which are derived as follows,

$$\xi(-h_0)=\frac{a_2-h_0}{a_2-a_3}=\frac{1}{2}-\frac{\sqrt{1-R}}{2}.$$

Given that $0<R<1$, we obtain $0<\xi(-h_0)<1/2$ by using the following equation

$$\xi(0)=\frac{a_2}{a_2-a_3}=\frac{1}{2}-\frac{z_m\sqrt{1-R}}{2\left(z_m+h_0\right)}.$$

$h_m<1/2$ implies that $1/2<\xi(0)<1$. Thus, in general, $0<|\xi(z)|<1$. Then, we derive the following relations

$$z+a_2=\xi(a_2-a_3),$$
$$z+a_3=(\xi-1)(a_2-a_3),$$
$$2z+a_2+a_3=(2\xi-1)(a_2-a_3),$$
$$\left(\frac{\partial U_0}{\partial z},\frac{\partial V_0}{\partial z}\right)=\frac{1}{a_2-a_3}\left(\frac{\partial\tilde{U}_0}{\partial\xi},\frac{\partial\tilde{V}_0}{\partial\xi}\right),$$
$$\left(\frac{\partial^2 U_0}{\partial z^2},\frac{\partial^2 V_0}{\partial z^2}\right)=\frac{1}{(a_2-a_3)^2}\left(\frac{\partial^2\tilde{U}_0}{\partial\xi^2},\frac{\partial^2\tilde{V}_0}{\partial\xi^2}\right).$$

Therefore, Eqs. (24) and (25) can be rewritten as follows,

$$\xi(1-\xi)\frac{\partial^2\tilde{U}_0}{\partial\xi^2}+(1-2\xi)\frac{\partial\tilde{U}_0}{\partial\xi}-\frac{i}{a_1\beta}\tilde{U}_0=-\frac{1}{a_1\beta}\frac{\partial N_0}{\partial x}, \quad (42)$$

$$\xi(1-\xi)\frac{\partial^2\tilde{V}_0}{\partial\xi^2}+(1-2\xi)\frac{\partial\tilde{V}_0}{\partial\xi}-\frac{i}{a_1\beta}\tilde{V}_0=-\frac{1}{a_1\beta}\frac{\partial N_0'}{\partial y}. \quad (43)$$

In these two equations, only the derivative $(\tilde{U}_0,\tilde{V}_0)$ of ξ exists. Thus, these equations can be regarded as ordinary differential equations. Notably, Eqs. (42) and (43) are hypergeometric equations, which can be solved analytically. The boundary conditions of these equations can be changed to the following forms accordingly.

$$\text{at}\quad \xi=\xi_0=\frac{a_2}{a_2-a_3},\quad \frac{\partial\tilde{U}_0(\xi)}{\partial\xi}=0,\quad \frac{\partial\tilde{V}_0(\xi)}{\partial\xi}=0, \quad (44)$$

$$\text{at}\quad \xi=\xi_h=\frac{a_2-h}{a_2-a_3},\quad \tilde{U}_0(\xi)=0,\quad \tilde{V}_0(\xi)=0. \quad (45)$$

The typical form of the hypergeometric equation is expressed as follows,

$$\xi(1-\xi)\frac{\mathrm{d}^2H(\xi)}{\mathrm{d}\xi^2}+\left[r-(a+b+1)\xi\right]\frac{\mathrm{d}H(\xi)}{\mathrm{d}\xi}-abH(\xi)=0. \quad (46)$$

In the present study, the parameters of Eqs. (42) and (43) are compared with those of Eq. (46) and the following relation can be derived,

$$\begin{cases} r=1 \\ a+b=1 \\ ab=i/(a_1\beta) \end{cases}. \quad (47)$$

The previously presented equations prove that $0<|\xi(z)|<1$. Thus, according to standard textbooks on special functions, such as that of Wang and Guo (2000), the two independent solutions to the homogeneous form of Eq. (46) around the singular point $\xi=0$ under the present parameter settings can be expressed as follows,

$$H_1(\xi)=\sum_{n=0}^{\infty}\frac{(a)_n(b)_n}{(1)_n n!}\xi^n, \quad (48)$$

$$H_2(\xi)=H_1(\xi)\ln\xi+\sum_{n=1}^{\infty}\frac{(a)_n(b)_n}{(1)_n n!}\xi^n\times \left[\psi(a+n)+\psi(b+n)-2\psi(1+n)-\psi(a)-\psi(b)+2\psi(1)\right]. \quad (49)$$

In Eqs. (48) and (49), $(\cdot)_n$ and ψ are defined as follows,

$$\begin{cases} (\lambda)_0=1 \\ (\lambda)_n=\lambda(\lambda+1)\cdots(\lambda+n-1)=\prod_{j=0}^{n-1}(\lambda+j),\ (n\geq1) \end{cases}, \quad (50)$$

and

$$\psi(z)=\frac{\mathrm{d}}{\mathrm{d}z}\ln\Gamma(z)=-\gamma-\frac{1}{z}+\sum_{n=1}^{\infty}\left(\frac{1}{n}-\frac{1}{z+n}\right), \quad (51)$$

where Γ is the Gamma function, expressed as follows,

$$\Gamma(z)=\frac{1}{z}\prod_{n=1}^{\infty}\left[\left(1+\frac{z}{n}\right)^{-1}\left(1+\frac{1}{n}\right)^{z}\right], \quad (52)$$

and γ is Euler's constant, expressed as follows,

$$\gamma=\lim_{n\to\infty}\left[\sum_{m=1}^{n}\frac{1}{m}-\ln n\right]. \quad (53)$$

According to Eqs. (47) and (50),

$$\begin{cases} n=0,\ (a)_0(b)_0=1 \\ n\geq1,\ (a)_n(b)_n=\left[\prod_{j=0}^{n-1}(a+j)\right]\left[\prod_{j=0}^{n-1}(b+j)\right] \\ \qquad\qquad =\prod_{j=0}^{n-1}(a+j)(b+j)=\prod_{j=0}^{n-1}\left(j^2+j+\frac{i}{a_1\beta}\right) \end{cases}. \quad (54)$$

Because $\psi(z)$ has the following relation,

$$\psi(z+n)=\psi(z)+\sum_{j=0}^{n-1}\frac{1}{z+j}, \quad (55)$$

then

$$\begin{aligned} &\psi(a+n)+\psi(b+n)-2\psi(1+n)-\psi(a)-\psi(b)+2\psi(1) \\ &=\psi(a)+\sum_{j=0}^{n-1}\frac{1}{a+j}+\psi(b)+\sum_{j=0}^{n-1}\frac{1}{b+j}- \\ &\quad 2\psi(1)-2\sum_{j=0}^{n-1}\frac{1}{1+j}-\psi(a)-\psi(b)+2\psi(1) \\ &=\sum_{j=0}^{n-1}\left(\frac{1}{a+j}+\frac{1}{b+j}-\frac{2}{1+j}\right) \\ &=\sum_{j=0}^{n-1}\left(\frac{1+2j}{j^2+j+i/(a_1\beta)}-\frac{2}{1+j}\right). \end{aligned} \quad (56)$$

Thus, Eqs. (48) and (49) can be rewritten as follows,

$$H_1(\xi)=1+\sum_{n=1}^{\infty}\left[\prod_{j=0}^{n-1}\left(j^2+j+\frac{i}{a_1\beta}\right)\frac{\xi^n}{(n!)^2}\right]=1+\sum_{n=1}^{\infty}b_n\xi^n, \quad (57)$$

$$\begin{aligned} H_2(\xi)&=H_1(\xi)\ln\xi+\sum_{n=1}^{\infty}\left[\prod_{j=0}^{n-1}\left(j^2+j+\frac{i}{a_1\beta}\right)\frac{\xi^n}{(n!)^2}\times\right. \\ &\quad \left.\sum_{j=0}^{n-1}\left(\frac{1+2j}{j^2+j+i/(a_1\beta)}-\frac{2}{1+j}\right)\right] \\ &=H_1(\xi)\ln\xi+\sum_{n=1}^{\infty}c_n\xi^n, \end{aligned} \quad (58)$$

where

$$b_n=\frac{1}{(n!)^2}\prod_{j=0}^{n-1}\left(j^2+j+\frac{i}{a_1\beta}\right),$$

$$c_n=\frac{1}{(n!)^2}\prod_{j=0}^{n-1}\left(j^2+j+\frac{i}{a_1\beta}\right)\times\sum_{j=0}^{n-1}\left(\frac{1+2j}{j^2+j+i/(a_1\beta)}-\frac{2}{1+j}\right).$$

Then, the solutions to the homogeneous forms of Eqs. (42) and (43) can be derived as follows,

$$\tilde{U}_0(x,y,\xi)=C_1H_1(\xi)+C_2H_2(\xi), \tag{59}$$

$$\tilde{V}_0(x,y,\xi)=C_3H_1(\xi)+C_4H_2(\xi), \tag{60}$$

where C_1 to C_4 are the integration constants, which are the functions of (x, y).

The acquisition of the special solutions to Eqs. (42) and (43) are trivial. Thus, the general solutions to Eqs. (42) and (43) have the following forms,

$$\tilde{U}_0(x,y,\xi)=C_1H_1(\xi)+C_2H_2(\xi)-i\frac{\partial N_0}{\partial x}, \tag{61}$$

$$\tilde{V}_0(x,y,\xi)=C_3H_1(\xi)+C_4H_2(\xi)-i\frac{\partial N_0'}{\partial y}. \tag{62}$$

Then, C_1 to C_4 can be determined by considering the surface and bottom conditions in Eqs. (44) and (45), as follows,

$$\begin{cases} C_1=i\dfrac{\partial N_0}{\partial x}A \\ C_2=i\dfrac{\partial N_0}{\partial x}B \\ C_3=i\dfrac{\partial N_0'}{\partial y}A \\ C_4=i\dfrac{\partial N_0'}{\partial y}B \end{cases}, \tag{63}$$

where

$$A=\frac{H_2'(\xi_0)}{H_2'(\xi_0)H_1(\xi_h)-H_1'(\xi_0)H_2(\xi_h)},$$

$$B=-\frac{H_1'(\xi_0)}{H_2'(\xi_0)H_1(\xi_h)-H_1'(\xi_0)H_2(\xi_h)}.$$

After the substitution of Eq. (63) into Eqs. (61) and (62), the solutions to Eqs. (42) and (43) can be derived, as follows,

$$\tilde{U}_0(x,y,\xi)=[AH_1(\xi)+BH_2(\xi)-1]i\frac{\partial N_0}{\partial x}=i\tilde{q}\frac{\partial N_0}{\partial x}, \tag{64}$$

$$\tilde{V}_0(x,y,\xi)=[AH_1(\xi)+BH_2(\xi)-1]i\frac{\partial N_0'}{\partial y}=i\tilde{q}\frac{\partial N_0'}{\partial y}, \tag{65}$$

where

$$\tilde{q}=AH_1(\xi)+BH_2(\xi)-1.$$

After reverse transformation of ξ to z, the solutions to Eqs. (24) and (25) can be rewritten as follows,

$$U_0(x,y,z)=iq\frac{\partial N_0}{\partial x}, \tag{66}$$

$$V_0(x,y,z)=iq\frac{\partial N_0'}{\partial y}, \tag{67}$$

where

$$q=AH_1(\xi(z))+BH_2(\xi(z))-1. \tag{68}$$

References

An, H. S., 1977. A numerical experiment of the M_2 tide in the Yellow Sea. *Journal of the Oceanographical Society of Japan*, **33**: 103-110.

Bowden, K. F., Fairbairn, L. A., and Hughes, P., 1959. The distribution of shearing stresses in a tidal current. *Geophysical Journal International*, **2** (4): 288-305.

Carbajal, N., and Backhaus, J. O., 1998. Simulation of tides, residual flow and energy budget in the Gulf of California. *Oceanologica Acta*, **21** (3): 429-446.

Chernetsky, A. S., Schuttelaars, H. M., and Talke, S. A., 2010. The effect of tidal asymmetry and temporal settling lag on sediment trapping in tidal estuaries. *Ocean Dynamics*, **60** (5): 1219-1241.

Choi, B. H., 1980. A tidal model of the Yellow Sea and the eastern China Sea. *Korea Ocean Research and Development Institute*, **80**: 42-43.

Davies, A. M., and Gerritsen, H., 1994. An intercomparison of three-dimensional tidal hydrodynamic models of the Irish Sea. *Tellus A*, **46** (2): 200-221.

Davies, A. M., Kwong, S. C. M., and Flather, R. A., 1997. Formulation of a variable-function three-dimensional model, with applications to the M_2 and M_4 tide on the North-West European Continental Shelf. *Continental Shelf Research*, **17** (2): 165-204.

Deng, F. J., Jiang, W. S., and Feng, S. Z., 2017. The nonlinear effects of the eddy viscosity and the bottom friction on the Lagrangian residual velocity in a narrow model bay. *Ocean Dynamics*, **67** (9): 1105-1118.

Ensing, E., de Swart, H. E., and Schuttelaars, H. M., 2015. Sensitivity of tidal motion in well-mixed estuaries to cross-sectional shape, deepening, and sea level rise: An analytical study. *Ocean Dynamics*, **65** (7): 933-950.

Fang, G. H., and Yang, J. F., 1985. A two-dimensional numerical model of the tidal motions in the Bohai Sea. *Chinese Journal of Oceanology and Limnology*, **3**: 135-152.

Fang, G. H., Yang, J. F., and Thao, Y. C., 1984. A two-dimensional numerical model for tidal motion in the Taiwan Strait. *Marine Geophysical Researches*, **7**: 267-276.

Guo, X. Y., and Yanagi, T., 1998. Three-dimensional structure of tidal current in the East China Sea and the Yellow Sea. *Journal of Oceanography*, **54** (6): 651-668.

Ianniello, J. P., 1977. Tidally induced residual currents in estuaries of constant breadth and depth. *Journal of Marine Research*, **35**: 755-786.

Jan, S., Wang, Y. H., Wang, D. P., and Chao, S. Y., 2004. Incremental inference of boundary forcing for a three-dimen-

sional tidal model: Tides in the Taiwan Strait. *Continental Shelf Research*, **24** (3): 337-351.

Jiang, W. S., and Feng, S. Z., 2014. 3D analytical solution to the tidally induced Lagrangian residual current equations in a narrow bay. *Ocean Dynamics*, **64** (8): 1073-1091.

Li, C. Y., 2001. 3D analytic model for testing numerical tidal models. *Journal of Hydraulic Engineering*, **127** (9): 709-717.

Li, C. Y., and Valle-Levinson, A., 1999. A two-dimensional analytic tidal model for a narrow estuary of arbitrary lateral depth variation: The intratidal motion. *Journal of Geophysical Research: Oceans*, **104**: 23525-23543.

Lu, Y. Y., and Lueck, R. G., 1999. Using a broadband ADCP in a tidal channel. Part II: Turbulence. *Journal of Atmospheric and Oceanic Technology*, **16** (11): 1568-1579.

Quan, Q., 2014. Application of the Lagrangian residual current theory to a model bay and the Xiangshan Bay. Master thesis. Ocean University of China (in Chinese with English abstract).

Ross, L., de Swart, H., Ensing, E., and Valle-Levinson, A., 2017. Three-dimensional tidal flow in a fjord-like basin with converging width: An analytical model. *Journal of Geophysical Research: Oceans*, **122** (9): 7558-7576.

Tee, K., 1979. The structure of three-dimensional tide-generating currents. Part I: Oscillating currents. *Journal of Physical Oceanography*, **9** (5): 930-944.

Wang, X. H., and Craig, P. D., 1993. An analytic model of tidal circulation in a narrow estuary. *Journal of Marine Research*, **51**: 447-456.

Wang, Z. X., and Guo, D. R., 2000. *An Introduction to Special Function*. Peking University Press, Beijing, 507pp.

Warner, J. C., Geyer, W. R., and Lerczak, J. A., 2005. Numerical modeling of an estuary: A comprehensive skill assessment. *Journal of Geophysical Research*, **110**: C5001.

Winant, C. D., 2007. Three-dimensional tidal flow in an elongated, rotating basin. *Journal of Physical Oceanography*, **37** (9): 2345-2362.

Xu, P., Liu, Z. Y., Mao, X. Y., and Jiang, W. S., 2013. Estimation of vertical eddy viscosity and bottom drag coefficients in tidally energetic narrow bay. *Periodical of Ocean University of China*, **43**: 1-7 (in Chinese with English abstract).

Xu, P., Mao, X. Y., and Jiang, W. S., 2016. Mapping tidal residual circulations in the outer Xiangshan Bay using a numerical model. *Journal of Marine Systems*, **154**: 181-191.

Xu, P., Mao, X. Y., and Jiang, W. S., 2017. Estimation of the bottom stress and bottom drag coefficient in a highly asymmetric tidal bay using three independent methods. *Continental Shelf Research*, **140**: 37-46.

(Edited by Xie Jun)